RSC Advances

PAPER

Cite this: *RSC Adv.*, 2016, **6**, 40033

Polymer blend nanocomposites based on poly(L-lactic acid), polypropylene and WS_2 inorganic nanotubes

Mohammed Naffakh,*[a] Ana M. Díez-Pascual[b] and Carlos Marco[c]

Received 4th March 2016
Accepted 13th April 2016

DOI: 10.1039/c6ra05803e

www.rsc.org/advances

Tungsten disulphide inorganic nanotubes (INT-WS_2) have been incorporated into poly(L-lactic acid) (PLLA)/polypropylene (PP) blends compatibilized with polypropylene-*grafted*-maleic anhydride (PP-*g*-MAH), and their effects on the morphology, thermal and mechanical properties of the resulting nanocomposites have been investigated. The nanofillers were uniformly dispersed at the nanoscale *via* a melt-blending process. The addition of 1.0 wt% INT-WS_2 to the PLLA/PP blends hardly affected their thermal stability or their degradation mechanism. Differential scanning calorimetry (DSC) thermograms revealed the nucleating role of INT-WS_2 on both polymeric components, reflected not only in an increase in the crystallization temperature from the melt but also in a rise in the crystallization enthalpy and the suppression of the cold-crystallization process; this effect was found to be more pronounced on PLLA and the blends rich in this component. Dynamic mechanical analysis (DMA) measurements demonstrated that the storage modulus of the nanocomposites was higher than those of the binary blends in the whole temperature range studied, ascribed to a synergistic effect of their increased crystallinity and the high INT-WS_2 rigidity. This study opens up new perspectives to develop novel INT-WS_2/polymer blend hybrid nanocomposites that show great potential for biomedical applications.

1. Introduction

Polymer blends have been widely used for several years and their market share is continuously growing. Unfortunately, because of the large unfavorable enthalpy of mixing, most polymer blends tend to macrophase separate, which leads to a deterioration in mechanical properties.[1] Therefore, controlling the phase behaviour and morphology becomes a key factor in converting these immiscible blends into useful products. In particular, nanocomposites that combine the renewable polymers and synthetic petroleum-based polymers along with the physical and chemical properties of nanoreinforcements find great potential in many applications, especially in packaging and biomedical sectors.[2]

Poly(L-lactic acid) (PLLA) is a biocompatible and environmentally friendly polymer that has attracted increasing attention in recent years as substitute of petroleum-based polymers.[3] However, PLLA also exhibits some disadvantages: its mechanical properties are not preserved at temperatures higher than the glass transition (60 °C), it has poor crystallizability that results in a long processing cycle time and a low production efficiency of products in the melt processing and molding. Blends of PLLA with several synthetic and biopolymers have been prepared in an effort to enhance the properties of PLLA.[4–7] Successful enhancement in the thermomechanical properties has been reported for PLLA/polypropylene (PP) blends compatibilized with graft copolymers such as polypropylene-*grafted*-maleic anhydride (PP-*g*-MAH).[8,9] Blending PP with PLLA has also been shown to be a simple and effective method to create a new material with better resistance to hydrolysis and lower price than neat PLLA, and better dyeability, sustainability and faster degradability than PP.[10]

Recently, several PLLA-based nanotechnologies have emerged with an emphasis on achieving chemical, mechanical, and biological properties superior to conventional biopolymers, opening a new dimension for the plastic industry. Therefore, these biopolymers have been formulated and associated with nano-sized fillers, which could bring a large range of improved properties (stiffness, permeability, crystallinity, thermal stability).[2] Along with many interesting nanofillers, inorganic fullerenes (IFs) and nanotubes (INTs) based on layered metal dichalcogenides, such as tungsten and molybdenum disulphide (WS_2/MoS_2), has become a field of recent interest.[10,11] The surprising properties of these nanostructures such as high impact resistance and superior tribological behaviour open up

[a]*Escuela Técnica Superior de Ingenieros Industriales, Universidad Politécnica de Madrid (ETSII-UPM), José Gutiérrez Abascal 2, 28006 Madrid, Spain. E-mail: mohammed.naffakh@upm.es*

[b]*Departamento de Química Analítica, Química Física e Ingeniería Química, Facultad de Biología, Ciencias Ambientales y Química, Universidad de Alcalá, 28871 Alcalá de Henares, Madrid, Spain*

[c]*Instituto de Ciencia y Tecnología de Polímeros (ICTP-CSIC), Juan de la Cierva 3, 28006 Madrid, Spain*

a wide variety of opportunities for applications in, for example, the automotive and aerospace industries, electronics and medical technology[12,13] and, more particularly, in the field of polymer nanocomposites.[14,15] Further, they exhibit much lower cytotoxicity than other nanoparticles, such as silica or carbon black.[16] Promising results have also been recently found with respect to the biocompatibility of INT(IF)-WS_2 with salivary gland cells.[17] With such excellent properties, and relatively simple and inexpensive fabrication, the incorporation of INT-WS_2 in biopolymer materials has become increasingly important (*i.e.* PPF, PLLA, PEEK).[18–20]

The present work explores an alternative strategy to prepare novel melt-processable (PLLA/PP) polymer blend nanocomposites based on the incorporation of small amounts of INT-WS_2, and the main objective is the analysis of their structure–property–performance relationship. In particular, we investigated the effect of INT-WS_2 on the processability, morphology, thermal and mechanical properties of the resulting new PLLA/PP/INT-WS_2 nanocomposites.

2. Experimental section

2.1. Materials and processing

Poly(L-lactic acid) (PLLA) and isotactic polypropylene (iPP) were purchased from Goodfellow Ltd. (density = 1.25 g cm^{-3}, $M_w \approx 1.5 \times 10^5$ g mol^{-1}) and Repsol-YPF ($d_{iPP} = 0.902$ g cm^{-3}, $M_{v,iPP} = 179 \times 10^3$ g mol^{-1}),[21] respectively. Multiwall WS_2 1D nanotubes (INT-WS_2) with diameters of 30–150 nm and lengths of 1–20 μm were obtained from NanoMaterials Ltd (Israel). A polypropylene-*graft*-maleic anhydride (PP-*g*-MA) with a maleic anhydride content of 0.42 wt% and a $M_v = 83.5 \times 103$ g mol^{-1} provided by EXXON was used as compatibilizer.

Both the compatibilized blends and nanocomposites were prepared following the same procedure: each mixture of PP, PP-*g*-MAH and PLLA, with or without INT-WS_2, was dispersed in a small volume of ethanol and homogenized by mechanical stirring and bath ultrasonication for approximately 15 min. Subsequently, the dispersion was partially dried in vacuum at 60 °C under a pressure of about 70 mbar for 24 h. The PLLA/$PP_{PP\text{-}g\text{-}MAH}$ blends are designated as 100/0, 90/10, 50/50, 90/10 and 0/100, where the numbers indicate the weight percentages of PLLA and $PP_{PP\text{-}g\text{-}MAH}$, respectively. The ratio between PP and PP-*g*-MAH was always 90 : 10. In the case of PLLA/$PP_{PP\text{-}g\text{-}MAH}$/INT-$WS_2$ nanocomposites, the INT-WS_2 fraction was 1.0 wt% of the total composite weight and the ratio of PLLA and $PP_{PP\text{-}g\text{-}MAH}$ was the same as in the binary blends [90/10-INT(89.1/9.9/1.0), 50/50-INT(49.5/49.5/1.0) and 10/90-INT(9.9/89.1/1.0)]. For the sake of comparison, reference samples of PLLA/INT-WS_2 (1.0 wt%) and $PP_{PP\text{-}g\text{-}MAH}$/INT-$WS_2$ (1.0 wt%) nanocomposites were also prepared in the same way. The melt-mixing of the resulting dispersions (~6 g) was performed using a conical micro twin-screw extruder (Thermo-Haake Minilab system) operating at 190 °C with a rotor speed of 100 rpm for 10 min. Then, the samples were pressed into films of 0.5 mm thickness in a hot press system using two heating/cooling plates. Efficient dispersion of the INT-WS_2 was achieved through using conventional, industrially viable processing methods: the most simple, cost-effective and ecologically friendly being the melt-processing route.

2.2. Characterization techniques

The morphology of the PLLA/$PP_{PP\text{-}g\text{-}MAH}$ blends and the PLLA/$PP_{PP\text{-}g\text{-}MAH}$/INT-$WS_2$ nanocomposites was characterized using an ultra-high field-emission scanning microscopy (FESEM) (SU8000, Hitachi Co., Japan). Cryogenically fractured surfaces from film specimens were coated with a ~5 nm Au/Pd layer to avoid charging during electron irradiation.

Wide-angle X-ray diffraction (WAXS) diffractograms were obtained using a Bruker D8 Advance diffractometer (Bruker AXS GmbH, Karlsruhe, Germany) employing Ni-filtered CuKα radiation ($\lambda = 1.5418$ Å), over the angular region 2θ between 5 and 40°. Compression moulded film samples were crystallized from the melt at 210 °C, at cooling rates of 10 °C min^{-1} in a Mettler FP90/FP82 HT temperature cell (Mettler-Toledo SAE, Barcelona, Spain).

The thermal stability of the nanocomposites was analyzed with a TA Instruments Q50 thermobalance between 100 and 800 °C, at a heating rate of 10 °C min^{-1} under an in inert (nitrogen) atmosphere. Experiments were carried out on samples with an average mass between 5 and 10 mg, with a purge gas flow rate of 60 ml min^{-1}. The parameters used for the evaluation of the results are the temperatures corresponding to 5 and 10% weight loss (T_5 and T_{10}), as well as the temperature and rate of maximum decomposition (T_{max} and R_{max}, respectively).

The crystallization and melting behaviour of the nanocomposites were investigated using a Perkin Elmer DSC7/7700 differential scanning calorimeter (Perkin-Elmer España SL, Madrid, Spain), calibrated with indium ($T_m = 156.6$ °C, $\Delta H_m = 28.45$ kJ kg^{-1}) and zinc ($T_m = 419.47$ °C, $\Delta H_m = 108.37$ kJ kg^{-1}). Samples of approximately 10 mg were studied in aluminium capsules under an inert nitrogen atmosphere with a flow rate of 25 ml min^{-1}. Under dynamic conditions cooling cycles from the melt were undertaken for each sample at two different cooling rates of 10 and 40 °C min^{-1}, followed by a heating cycle at 5 °C min^{-1} from 40 to 210 °C. Prior to cooling/heating, the samples were held at 210 °C for 5 min to erase any thermo-mechanical memory effects. The melting temperature (T_m) and the crystallization temperature (T_p) were determined at the maximum of the melting endotherm observed during the heating scan and the minimum of the crystallization exotherm observed during the cooling scan, respectively.

Dynamic mechanical experiments were performed on rectangular shaped samples using a Mettler DMA 861 device, in the tensile mode at frequencies of 1 Hz. A dynamic force of 6 N oscillating at fixed frequency and amplitude of 30 μm was used. The relaxation spectra were recorded over the temperature range −100 to 100 °C, at a heating rate of 2 °C min^{-1}.

3. Results and discussion

3.1. Morphology

PLLA and PP polymers are reported to have poor compatibility,[22] and incompatible polymers will be phase separated when mixed

together. To solve this problem, PP-*g*-MAH has been used in this work as an additive to improve the compatibility of immiscible PLLA/PP blends. The presence of PP-*g*-MAH would improve the compatibility of PLLA/PP blends since the PP part of PP-*g*-MA is compatible with the PP and the active site in the anhydride group reacts with the carbonyl group of PLLA resulting in an ester linkage.[9] However, to further expand its range of practical applications, new strategies are required like blending PLLA/PP with nano-fillers in order to attain optimal performance. In this way, one promising approach for the fabrication of hybrid biopolymer composites is the incorporation of INT-WS_2. Fig. 1 shows the SEM morphologies of the raw INT-WS_2 and cryogenically-fractured surfaces of different compositions of PLLA/$PP_{PP\text{-}g\text{-}MAH}$ and PLLA/$PP_{PP\text{-}g\text{-}MAH}$/INT-$WS_2$ obtained at low and high magnifications. The micrograph of 90/10 blend reveals a distinct two phase morphology with the PP phase dispersed evenly within the PLLA matrix. The presence of PP-*g*-MAH is expected to reduce the interfacial tension between PLLA and PP. However, no morphological evidence of good adhesion between the matrix and the dispersed phase can be seen. Moreover, the apparent particle size (*i.e.* mean diameter) seem to increase with increasing PP content. Above 50/50 wt% (PLLA/$PP_{PP\text{-}g\text{-}MAH}$) blend, the morphology is reversed (*i.e.* when PLLA concentration is less than 50 wt%, PLLA becomes the dispersed phase in PP). Analogously, SEM was also used to obtain high-resolution images of the ternary PLLA/$PP_{PP\text{-}g\text{-}MAH}$/INT hybrid nanocomposites in order to observe the dispersion of the INT-WS_2 within the PLLA/$PP_{PP\text{-}g\text{-}MAH}$ blends (Fig. 1). In particular, it was found that the processing of the PLLA/$PP_{PP\text{-}g\text{-}MAH}$/INT-$WS_2$ nanocomposites was effective with the INTs uniformly dispersed at the nanoscale by the shear force encountered during melt-blending, without forming aggregates or agglomerates. This strategy yields finer dispersion, with the INT-WS_2 almost fully debundled into individual tubes (see the arrows marked on the image). A similar effect was observed for both PLLA/INT and $PP_{PP\text{-}g\text{-}MAH}$/INT nanocomposites. In addition, the images of PLLA/$PP_{PP\text{-}g\text{-}MAH}$/INT also suggest that the phase boundary between the PLLA and $PP_{PP\text{-}g\text{-}MAH}$ constituents was modified by the INTs. This phenomenon was primarily due to the reinforcing effect of INTs, which contributed to an effective stress transfer to the matrix at the interface (*i.e.* 90/10-INT). More importantly, a reduction of the dispersed phase particles can be seen for the PLLA/$PP_{PP\text{-}g\text{-}MAH}$/INT-$WS_2$ nanocomposites compared to those in the blends without INT-WS_2. This is because the efficient dispersion and localization of the INTs at the matrix-dispersed phase interface may form a solid barrier that inhibits or prevents the coalescence of the drops.

3.2. Thermal stability

The values of the thermal parameters associated to the thermal stability of the blends and nanocomposites developed in this work are listed in Table 1. Fig. 2a presents the weight loss as a function of temperature for PLLA/$PP_{PP\text{-}g\text{-}MAH}$ blends, confirming the higher thermal stability of $PP_{PP\text{-}g\text{-}MAH}$, $T_5 = 400.6$ °C, compared to PLLA, $T_5 = 341.7$ °C. The addition of $PP_{PP\text{-}g\text{-}MAH}$ to PLLA hardly increases the thermal stability of the biopolymer, and the thermal degradation of both components takes place *via* different mechanisms, since two well defined decomposition stages can be observed. In this regard, Fig. 2b presents derivative thermogravimetric (DTG) curves associated with the thermal degradation, showing two maxima in the decomposition rate, each of them related to each of the blend components. Our results are consistent with previous studies on PP/PLA blends, where the addition of 10 wt% PP had negligible effect on the thermal stability of PLLA.[23] Although the change in T_{max} values is small, except for the mixture with the highest PLLA content (Fig. 3a), the change in the corresponding values of maximum rate of decomposition is representative of the variation in the composition of the blends, Fig. 3b.

The addition of 1.0 wt% INT-WS_2 to the PLLA/$PP_{PP\text{-}g\text{-}MAH}$ blends hardly affects the thermal stability, except for a slight increase in the case of samples rich in $PP_{PP\text{-}g\text{-}MAH}$, Table 1, without apparent perturbation of the mechanisms of degradation of the blend components, as can be deduced from the presence of the degradation maxima corresponding to $PP_{PP\text{-}g\text{-}MAH}$ and PLLA discussed previously (see Fig. 4).

3.3. Crystallization behaviour

Fig. 5a shows the cooling thermograms from the melt of raw PLLA, $PP_{PP\text{-}g\text{-}MAH}$ and the PLLA/$PP_{PP\text{-}g\text{-}MAH}$ blends at a rate of 10 °C min^{-1}. As it can be observed, the crystallization exotherms shift to lower temperatures and present lower enthalpy as the concentration of PLLA in the blend increases. It is noteworthy that the crystallization exotherm of neat PLLA is difficult to be detected, with a crystallization enthalpy of only 8.0 J g^{-1}. Analogously, Fig. 5b compares the thermograms of the nanocomposites with 1.0 wt% INT-WS_2 at the same cooling rate, showing a shift of the crystallization exotherms towards higher temperatures and an increase in the enthalpy of neat PLLA, up to 49.9 J g^{-1}. For comparative purposes, Fig. 6 displays the variation of T_c *vs.* PLLA concentration, at a cooling rate of 10 °C min^{-1}, both for the PLLA/$PP_{PP\text{-}g\text{-}MAH}$ blends and for the corresponding nanocomposites with INT-WS_2. Regarding the blends, a slight rise in the crystallization temperature is found upon increasing $PP_{PP\text{-}g\text{-}MAH}$ content, from 93.3 °C for neat PLLA to 116.4 °C for raw $PP_{PP\text{-}g\text{-}MAH}$. A noticeable increase up to 107.2 °C is already found in the 90/10 wt% (PLLA/$PP_{PP\text{-}g\text{-}MAH}$) blend, while the increment becomes smaller at higher $PP_{PP\text{-}g\text{-}MAH}$ concentrations. The presence of 1.0 wt% INT-WS_2 causes an increase in the crystallization temperature, both in the neat polymers and in the blends, the rise being higher than 20 °C for the neat PLLA and about 6 °C for the neat $PP_{PP\text{-}g\text{-}MAH}$, see Table 2. This phenomenon can also be observed in the nanocomposites, albeit in this case it seems not to be dependent on the concentration of the components. Nonetheless, the rise in T_c for PLLA/$PP_{PP\text{-}g\text{-}MAH}$/INT-$WS_2$ (90/10-INT) compared to the corresponding PLLA/$PP_{PP\text{-}g\text{-}MAH}$ blend is higher than 13 °C, while for the (10/90-INT) nanocomposite the increase is about 9 °C. These results suggest the existence of a nucleating effect of the nanofiller on both polymeric components, the effect being more pronounced on PLLA and the blends rich in this component. It should be noticed that, in the case of the 50/50-INT nanocomposite,

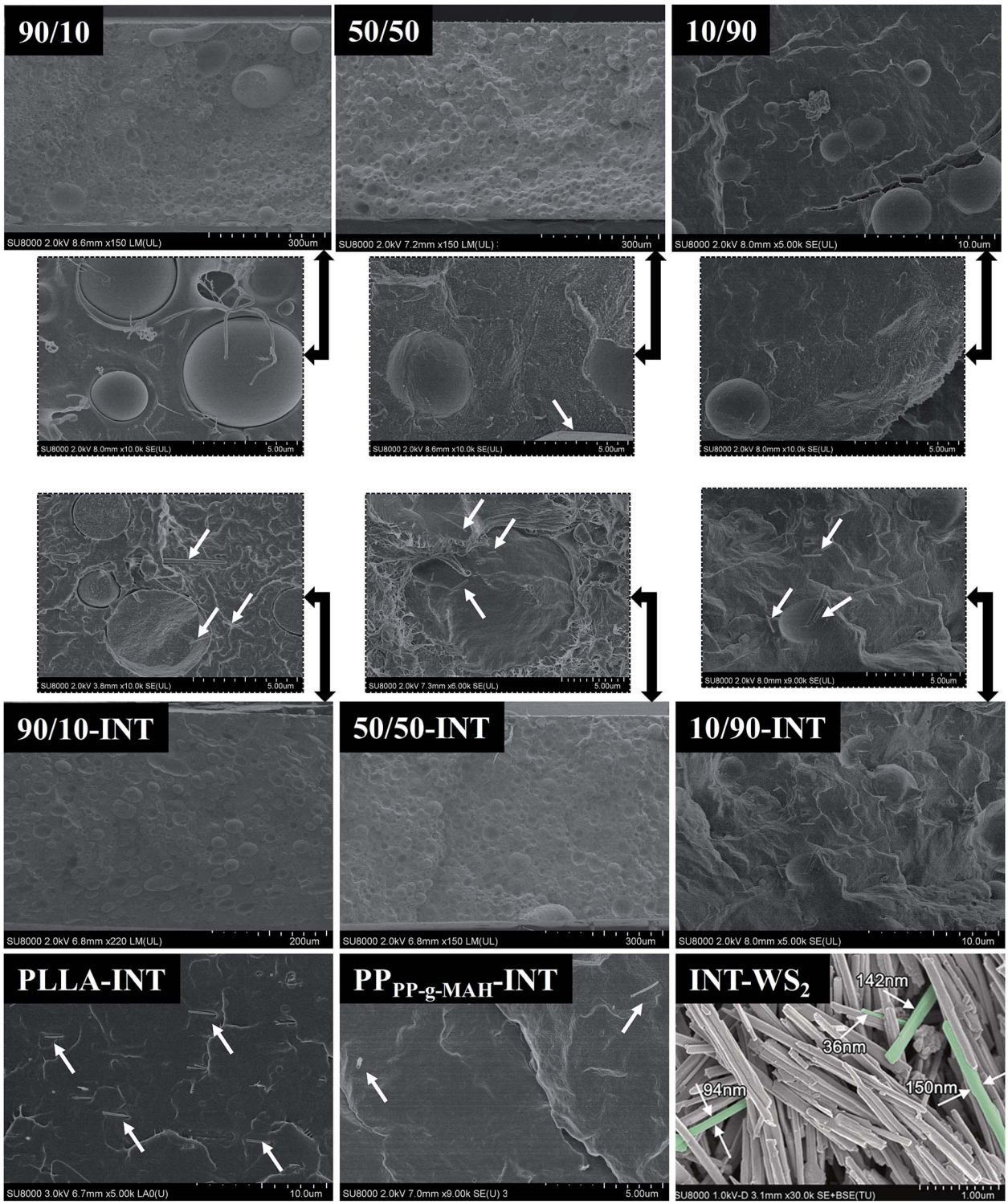

Fig. 1 Low and high magnification SEM images for raw INT-WS_2, PLLA/INT-WS_2, $PP_{PP\text{-}g\text{-}MAH}$/INT-$WS_2$, binary PLLA/$PP_{PP\text{-}g\text{-}MAH}$ and ternary PLLA/$PP_{PP\text{-}g\text{-}MAH}$/INT-$WS_2$ nanocomposites. The micrographs highlight the nanotube dimensions (diameter) and their distribution within the samples (marked with white arrows on the images).

a double crystallization exotherm is found, Fig. 5b, with T_c values of 112.1 °C and 121.8 °C, which could be related to the existence of two macrophases in the nanocomposite, one incorporating almost 1.0 wt% INT-WS_2 and other with hardly amount of nanofiller. This phenomenon can also be observed when the cooling rate increases up to 40 °C min^{-1}.

It is very important to note that the abovementioned nucleating effect, reflected in an increase in the crystallization

Table 1 TGA parameters of different PLLA/$PP_{PP\text{-}g\text{-}MAH}$/INT-$WS_2$ blend nanocomposites based on PLLA, $PP_{PP\text{-}g\text{-}MAH}$ and INT-WS_2[a]

Material	T_5 (°C)	T_{10} (°C)	T_{max} (°C)	R_{max} (% °C^{-1})
PLLA	341.7	351.6	381.6	2.80
PLLA-INT	340.5	349.8	377.1	2.99
90/10	326.6	342.5	377.9–433.4	2.16–0.41
90/10-INT	326.1	341.3	371.9–462.6	2.22–0.49
50/50	340.3	354.2	374.9–464.8	1.23–1.12
50/50-INT	349.3	374.0	362.9–473.1	0.25–2.05
10/90	346.2	376.9	359.1–471.6	0.21–1.83
10/90-INT	349.3	374.0	362.1–472.3	0.25–2.06
$PP_{PP\text{-}g\text{-}MAH}$	400.6	473.1	473.1	2.18
$PP_{PP\text{-}g\text{-}MAH}$-INT	408.8	425.8	471.6	2.43

[a] T_5: temperature for 5% weight loss; T_{10}: temperature for 10% weight loss; T_{max}: temperature corresponding to the maximum rate of weight loss and R_{max}: rate of maximum decomposition.

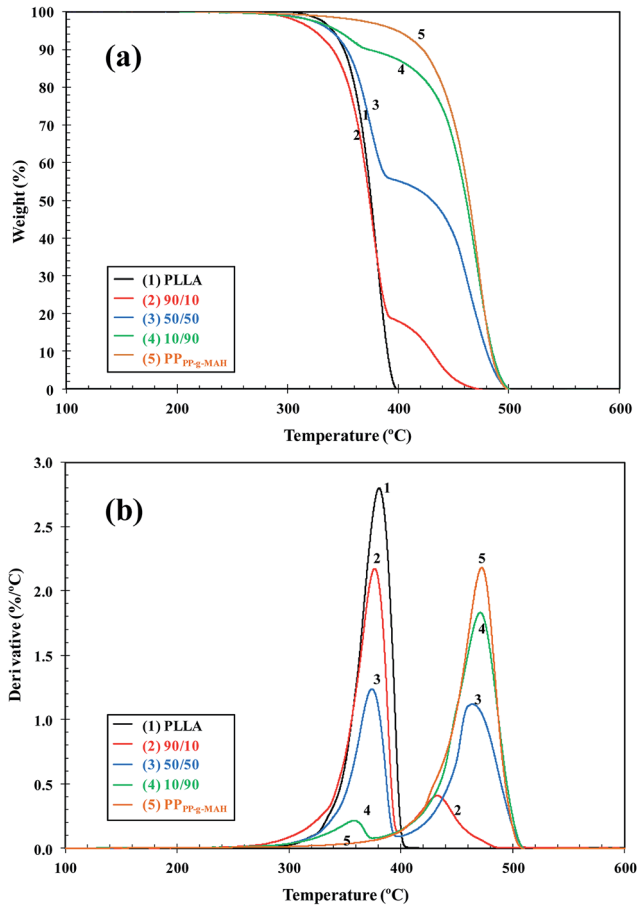

Fig. 2 (a) Thermogravimetric (TGA) and (b) derivative thermogravimetric (DTG) curves of PLLA/$PP_{PP\text{-}g\text{-}MAH}$ blends.

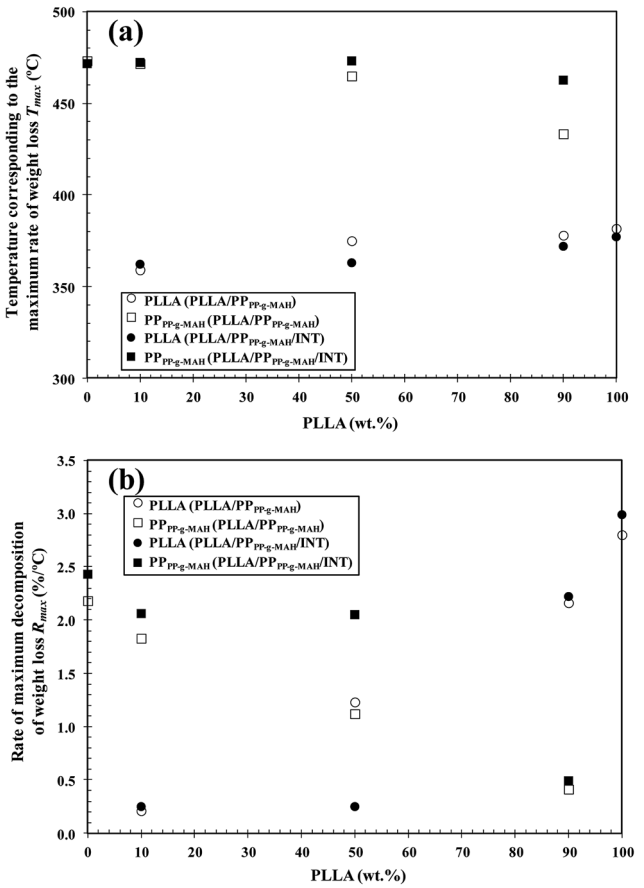

Fig. 3 (a) Variation of the temperature and (b) rate of maximum decomposition (T_{max}/R_{max}) of PLLA and $PP_{PP\text{-}g\text{-}MAH}$ in the binary PLLA/$PP_{PP\text{-}g\text{-}MAH}$ and ternary PLLA/$PP_{PP\text{-}g\text{-}MAH}$/INT-$WS_2$ nanocomposites with composition.

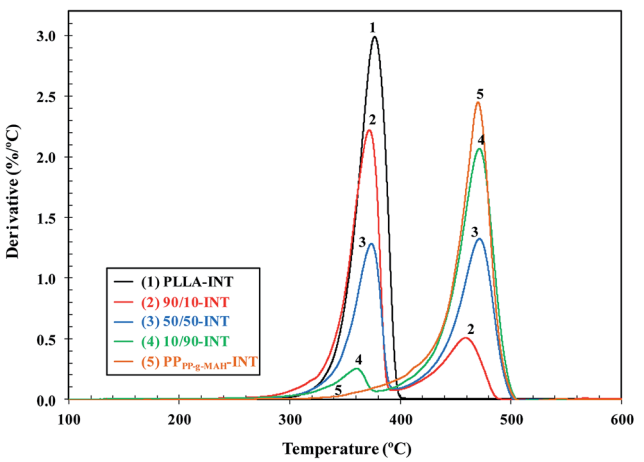

Fig. 4 DTG curves of PLLA-INT, $PP_{PP\text{-}g\text{-}MAH}$-INT and different ternary PLLA/$PP_{PP\text{-}g\text{-}MAH}$/INT-$WS_2$ nanocomposites.

temperature, becomes particularly interesting when analyzing the crystallization enthalpy behaviour. Thus, Fig. 7 shows the variation of the crystallization enthalpy (ΔH_c) for the blends and the nanocomposites, and the crystallization parameters obtained are collected in Table 2. Regarding the blends without nanofiller, a strong reduction in ΔH_c is found, from 91.1 J g^{-1} for $PP_{PP\text{-}g\text{-}MAH}$, that is, 43.9% crystallinity considering a value of enthalpy of melting for perfect crystals ΔH_{100} ($PP_{PP\text{-}g\text{-}MAH}$) = 207.1 J g^{-1} (ref. 24) to 8 J g^{-1} for PLLA, which corresponds to 8.6% crystallinity taking a value of ΔH_{100} (PLLA) = 93 J g^{-1}.[25]

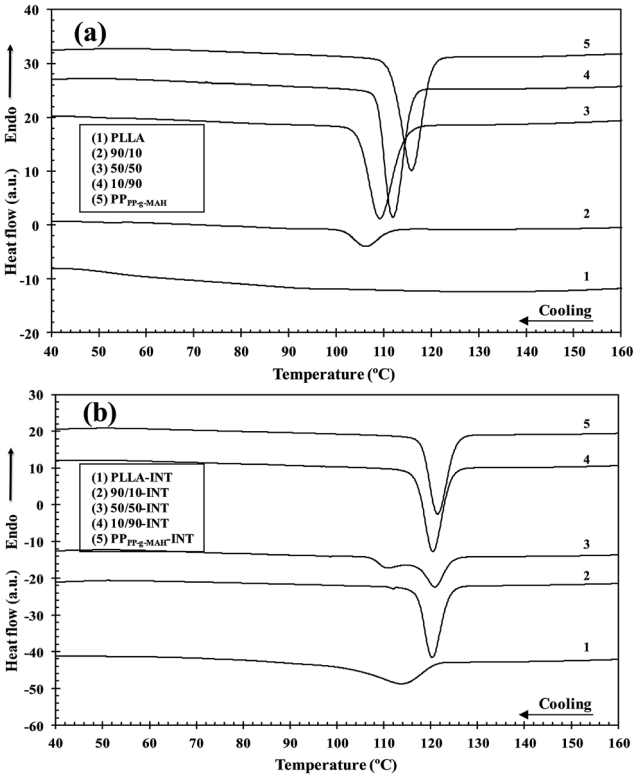

Fig. 5 DSC thermograms of the dynamic crystallization of PLLA, $PP_{PP\text{-}g\text{-}MAH}$, binary PLLA/$PP_{PP\text{-}g\text{-}MAH}$ and ternary PLLA/$PP_{PP\text{-}g\text{-}MAH}$/INT-$WS_2$ nanocomposites obtained during cooling from the melt to room temperature at 10 °C min^{-1}.

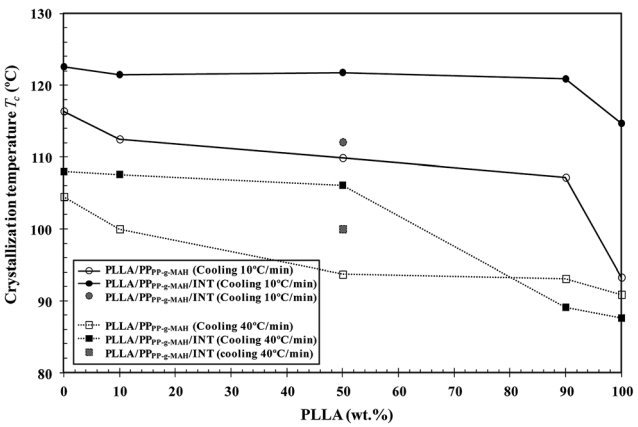

Fig. 6 Variation of the crystallization temperature (T_c) of PLLA and $PP_{PP\text{-}g\text{-}MAH}$ in the binary PLLA/$PP_{PP\text{-}g\text{-}MAH}$ and ternary PLLA/$PP_{PP\text{-}g\text{-}MAH}$/INT-$WS_2$ nanocomposites with composition at the indicated cooling rates.

Regarding the nanocomposites, a remarkable increase in ΔH_c is observed due to the nucleating effect of INT-WS_2, up to 49.9 J g^{-1} (53.7% crystallinity) and 105.4 J g^{-1} (50.9%) crystallinity for neat PLLA and $PP_{PP\text{-}g\text{-}MAH}$, respectively, and it is slightly higher for the nanocomposites with 50 and 90% PLLA.

It is well known and widely described in the literature that PLLA loses crystallization ability from the melt as the cooling rate increases. Depending on polymer molecular weight, amongst other factors, PLLA may not be able to crystallize in the cooling cycles form the melt at rates higher than 5 °C min^{-1}, leading to an amorphous–crystal transition during the subsequent heating cycles, process known as "cold-crystallization".[26,27] This process is mainly related to the increase in the mobility of the PLLA chain segments during the heating at a temperature somewhat higher compared to that reached during the cooling process, which favors both the nucleation step and the crystal growth. As mentioned previously, in this work neat PLLA only develops a crystallinity of about 8.0% during the cooling process at a rate of 10 °C min^{-1} and reaches a crystallinity of 30% during the subsequent heating cycle. The 50/50 and 90/10 PLLA/$PP_{PP\text{-}g\text{-}MAH}$ blends, which crystallize from the melt with enthalpy values of 53.9 and 17.8 J g^{-1}, respectively, also exhibit this cold crystallization behaviour, albeit it is less pronounced than in the neat PLLA, with cold-crystallization enthalpy values (ΔH_{cc}) of 8.6 and 24.2 J g^{-1}, Fig. 7. Regarding the nanocomposites, the crystallinity developed by PLLA/INT-WS_2 is about 53.7%, and no cold-crystallization process is detected during the subsequent crystallization. The same behaviour is found for all the blends with $PP_{PP\text{-}g\text{-}MAH}$ (Fig. 7 and Table 2). Clearly, the presence of the nanofiller causes an increase in the nucleation rate, hence, and increase in the overall crystallization rate, reflected not only in an increase in the crystallization temperature from melt but also in a rise in the crystallization enthalpy and the suppression of the cold-crystallization process.

As mentioned above, the presence and magnitude of the PLLA cold-crystallization process is strongly dependent on the cooling rate. In other series of experiments, the cooling rate from the melt was increased up to 40 °C min^{-1} for all the samples (Fig. 8a and b). As can be observed in Fig. 6, the increase in the cooling rate remarkably decreases the T_c both in the blends and in the nanocomposites, the reduction being more dependent on the composition than in the case of cooling at 10 °C min^{-1}. In contrast, the increase in the cooling rate does not significantly affect the ΔH_c of PLLA/$PP_{PP\text{-}g\text{-}MAH}$ blends, which exhibit similar behaviour to that found for the crystallization at 10 °C min^{-1}, while for the nanocomposites the developed enthalpy is lower (Table 2) the drop being stronger for the 90/10-INT sample, which enthalpy is reduced to only 20.5 J g^{-1}, and for PLLA/INT-WS_2, which hardly crystallizes with an enthalpy of only 3.3 J g^{-1}, about 3.5% crystallinity. Accordingly, these two nanocomposites show cold-crystallization during the subsequent heating, with cold crystallization temperatures (T_{cc}) values of 84.9 and 88.2 °C, developing enthalpies of 16.4 and 32.4 J g^{-1}, respectively. As discussed earlier, the presence of the nanofiller considerably modifies the crystallization behaviour of both the neat components and the blends, provoking an increase in the nucleating rate during the cooling process from the melt, favouring the formation of crystalline nucleus at higher crystallization temperatures, therefore, at lower sub-coolings, phenomenon that is considerably more pronounced for PLLA and the nanocomposites rich in this component, in which the cold-crystallization behaviour is significantly modified, as will be discussed later. Nucleating effects due to the

Table 2 DSC parameters of different PLLA/$PP_{PP\text{-}g\text{-}MAH}$/INT-$WS_2$ blend nanocomposites based on PLLA, $PP_{PP\text{-}g\text{-}MAH}$ and INT-WS_2[a]

	Cooling at 10 °C min^{-1}		Subsequent heating at 10 °C min^{-1}				Cooling at 40 °C min^{-1}		Subsequent heating at 10 °C min^{-1}			
Material	T_c (°C)	ΔH_c (J g^{-1})	T_{cc} (°C)	ΔH_{cc} (J g^{-1})	T_m (°C)	ΔH_m (J g^{-1})	T_c (°C)	ΔH_c (J g^{-1})	T_{cc} (°C)	ΔH_{cc} (J g^{-1})	T_m (°C)	ΔH_m (J g^{-1})
PLLA	93.3	8.0	104.1	27.9	166.0	47.4	90.9	4.4	91.4	36.9	137.2 151.3	39.5
PLLA-INT	114.7	49.9	—	—	155.5 161.0	50.2	87.6	3.3	88.2	32.4	143.3 155.1	41.6
90/10	107.2	17.8	87.9	24.2	148.2 159.2	45.1	93.1	15.3	88.4	29.2	145.0 155.6 161.9	47.3
90/10-INT	120.9	54.3	—	—	162.1	52.7	89.1	20.5	84.9	16.4	148.0 155.4 162.9	59.3
50/50	109.9	53.9	88.4	27.9	155.6 165.4	56.9	93.7	51.1	87.1	14.6	152.7 163.0	60.4
50/50-INT	112.1 121.8	67.8	—	—	160.0 164.8	55.1	100.0 106.1	57.4	—	—	159.0 163.3	62.4
10/90	112.5	84.4	—	—	155.6 164.0	64.2	100.0	82.8	—	—	155.0 162.0	69.1
10/90-INT	121.5	91.5	—	—	161.6	65.6	107.6	81.7	—	—	157.6 162.5	69.3
$PP_{PP\text{-}g\text{-}MAH}$	116.4	91.1	—	—	155.4 163.9	65.6	104.5	88.1	—	—	153.3 162.0	77.3
$PP_{PP\text{-}g\text{-}MAH}$-INT	122.6	105.4	—	—	161.4	68.3	108.0	89.2	—	—	158.9 162.9	77.7

[a] T_c: crystallization temperature; ΔH_c: crystallization enthalpy; T_{cc}: cold-crystallization temperature; ΔH_{cc}: cold-crystallization enthalpy; T_m: melting temperature; ΔH_m: melting enthalpy.

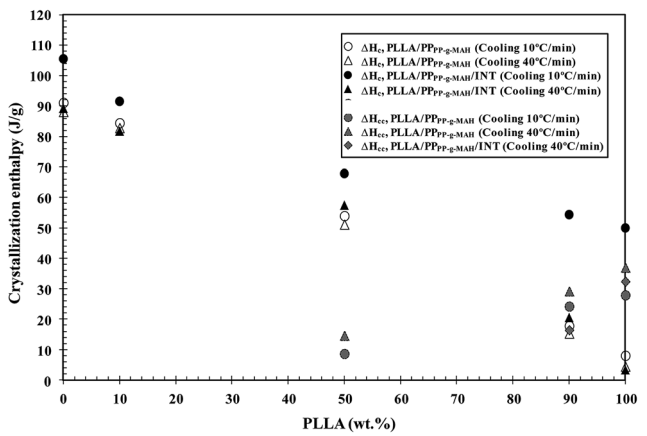

Fig. 7 Variation of both crystallization enthalpy (ΔH_c) and cold-crystallization enthalpy (ΔH_{cc}) of PLLA and $PP_{PP\text{-}g\text{-}MAH}$ in the binary PLLA/$PP_{PP\text{-}g\text{-}MAH}$ and ternary PLLA/$PP_{PP\text{-}g\text{-}MAH}$/INT-$WS_2$ nanocomposites with composition at the indicated cooling rates.

presence of nanofillers have been previously reported for PP reinforced with inorganic fullerenes inorganic nanotubes, carbon nanotubes, and nanoclays[14] and also for PLLA filled with inorganic nanotubes, nano-calcium carbonate, nano-zinc citrate, graphene oxide and fullerenes (C60), nanoclay and carbon nanotubes.[19] In particular, it was shown that INT-WS_2 exhibits much more prominent nucleation activity on the crystallization of PLLA than other specific nucleating agents or nano-sized fillers.[19]

3.4. Melting behaviour

Fig. 9a compares the heating thermograms after cooling from the melt at 10 °C min^{-1} of PLLA/$PP_{PP\text{-}g\text{-}MAH}$ blends with those of neat PLLA and $PP_{PP\text{-}g\text{-}MAH}$. As it can be observed, after the exotherm related to the aforementioned cold-crystallization process, neat PLLA shows a main endotherm with a maximum at 166.0 °C and a shoulder at around 152 °C. The X-ray diffractogram of this sample (see Fig. 10), crystallized under the same conditions, does not show polymorphism, indicating the only existence of the α-form of PLLA (*i.e.* strongest visible diffraction peak of the (200)/(110) plan at 16.7°).[19,28,29] According to these results, the shoulder could be associated to the melting of PLLA crystals originated during the cooling process from the melt, while the endotherm at 166.0 °C likely corresponds to those generated by cold-crystallization during the heating, albeit could also be related to melting–recrystallization–melting processes (*i.e.* reorganization of all crystals).[19] In the same way, the appearance of the scattering intensity profile of neat $PP_{PP\text{-}g\text{-}MAH}$, (110) at $2\theta = 14.2°$, (040) at 17.0° and (130) at 18.6° and overlapping (131) and (111) at 21.3° and 21.9° related to the principal reflections of the α-crystals[30] (Fig. 10) suggests that the second endothermic peak arises from the rearrangement of the initial crystal morphology (*i.e.* melting–recrystallization–

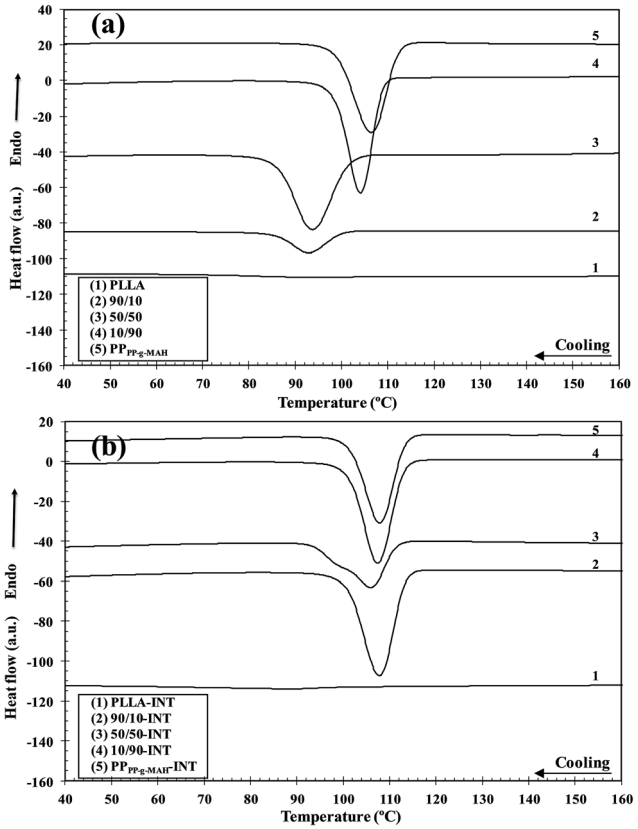

Fig. 8 DSC thermograms of the dynamic crystallization of PLLA, $PP_{PP\text{-}g\text{-}MAH}$, binary PLLA/$PP_{PP\text{-}g\text{-}MAH}$ and ternary PLLA/$PP_{PP\text{-}g\text{-}MAH}$/INT-$WS_2$ nanocomposites obtained during cooling from the melt to room temperature at 40 °C min^{-1}.

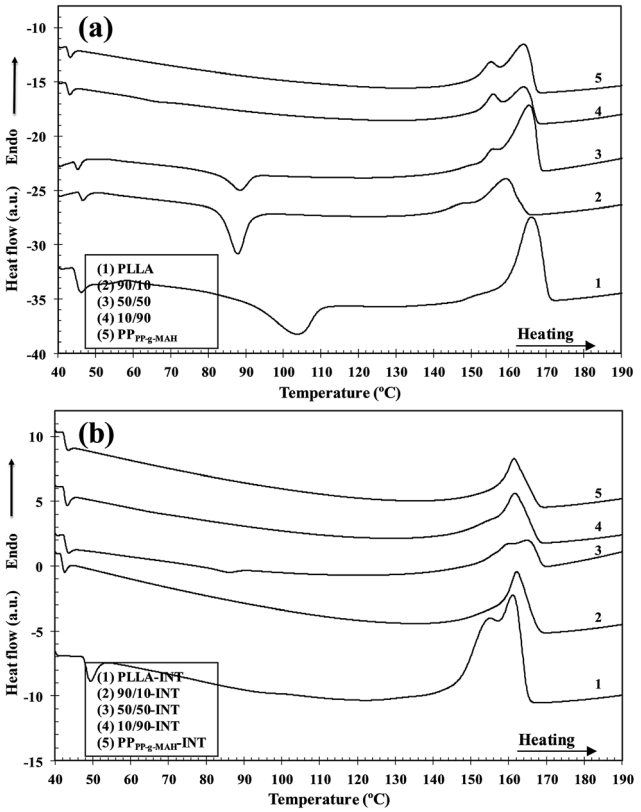

Fig. 9 DSC thermograms of melting of PLLA, $PP_{PP\text{-}g\text{-}MAH}$, binary PLLA/$PP_{PP\text{-}g\text{-}MAH}$ and ternary PLLA/$PP_{PP\text{-}g\text{-}MAH}$/INT-$WS_2$ nanocomposites obtained during heating at 10 °C min^{-1} after cooling from the melt to room temperature at 10 °C min^{-1}.

melting) and that the first endothermic peak represents the melting of original crystals formed when the $PP_{PP\text{-}g\text{-}MAH}$ sample was cooled from the melt. The increase of $PP_{PP\text{-}g\text{-}MAH}$ concentration in the blends decreases the temperature and enthalpy associated to the cold-crystallization, and also makes more pronounced the double endotherm phenomenon. Regarding the 90/10 binary blend, an important reduction of the maxima of both endotherms is detected compared to neat PLLA, which could be related to the decrease in T_{cc}, which originates smaller and more imperfect lamellae. When the concentration of $PP_{PP\text{-}g\text{-}MAH}$ increases up to 50%, the double endotherm shifts to higher temperatures. In particular, the endotherm at higher temperature (165.4 °C) should be ascribed to the overlapping of the melting of α-monoclinic crystals of $PP_{PP\text{-}g\text{-}MAH}$ and the orthorhombic crystals of the α-form of PLLA. Regarding the 10/90 blend, the first endothermic peak of $PP_{PP\text{-}g\text{-}MAH}$ becomes more pronounced, and hardly changes for neat $PP_{PP\text{-}g\text{-}MAH}$.

The WAXS diffractograms of the binary and ternary hybrid nanocomposites are shown in Fig. 10. A new diffraction intensity is detected compared to neat $PP_{PP\text{-}g\text{-}MAH}$, which could be related to a small fraction of $PP_{PP\text{-}g\text{-}MAH}$ β-trigonal crystals (*i.e.* weak diffraction peak of the (300) plane at about 16).[30–33] Consequently, the formation of the endotherm at higher temperature of $PP_{PP\text{-}g\text{-}MAH}$ in the PLLA/$PP_{PP\text{-}g\text{-}MAH}$ blends could be attributed to the melting of $PP_{PP\text{-}g\text{-}MAH}$ crystals originated both from the β/α transformation processes and from the melting–recrystallization–melting in $PP_{PP\text{-}g\text{-}MAH}$.[32,33] However, no structural evidence of the increase of the principal reflection of β-crystals with PLLA concentration can be observed. Thus, the formation of the β-crystals could be induced by the experimental procedure used for the preparation of these compressed films (*i.e.* the hot-stage cell, see Section 2.2) rather than the presence of PLLA. In addition, the WAXS diffractograms of the ternary hybrid nanocomposites only show the abovementioned characteristic reflections of the PLLA and $PP_{PP\text{-}g\text{-}MAH}$, demonstrating that the INT-WS_2 does not influence the crystal structure of the PLLA/$PP_{PP\text{-}g\text{-}MAH}$ polymer blends. The appearance of a scattering intensity profile in PLLA/INT-WS_2 at $2\theta = 14.5°$ is related the principal reflection (002) of the INT-WS_2.[34] However, in the case of the ternary PLLA hybrid nanocomposites, this characteristic diffraction of the INT-WS_2 is masked by the presence of the strong diffraction peak of the α-crystals of $PP_{PP\text{-}g\text{-}MAH}$.

The addition of 1.0 wt% INT-WS_2 to the PLLA/$PP_{PP\text{-}g\text{-}MAH}$ blends considerably modifies the melting behaviour (see Fig. 9b). On the one hand, the heterogeneous nucleating effect suppresses the cold-crystallization processes, since it causes an increase in the nucleation rate and in the number of crystalline nuclei during the crystallization from the melt, and on the other

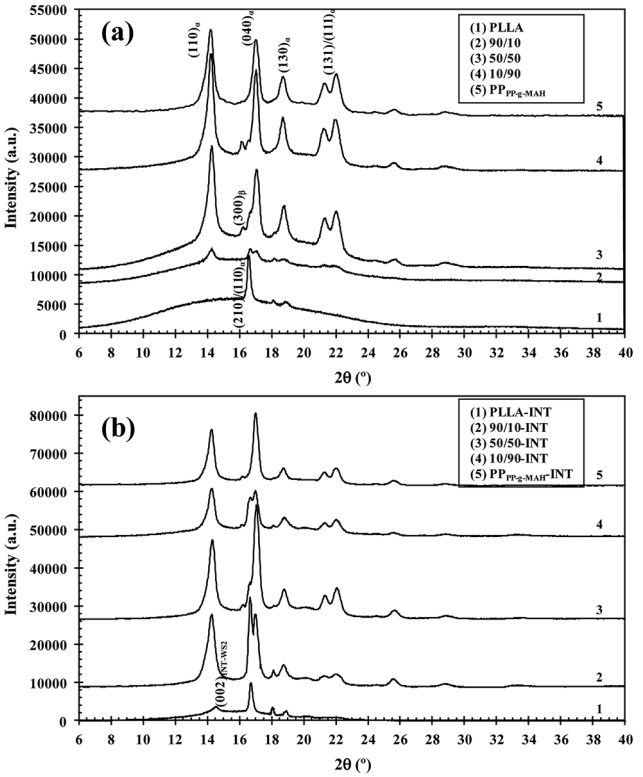

Fig. 10 WAXS diffractograms of PLLA, $PP_{PP\text{-}g\text{-}MAH}$, binary PLLA/$PP_{PP\text{-}g\text{-}MAH}$ and ternary PLLA/$PP_{PP\text{-}g\text{-}MAH}$/INT-$WS_2$ nanocomposites obtained during cooling from the melt to room temperature at 10 °C min^{-1}.

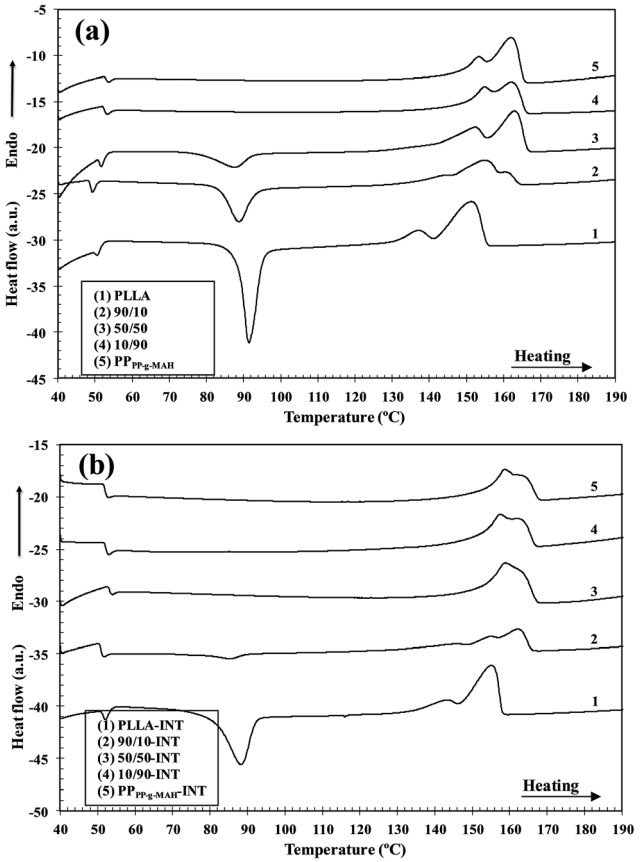

Fig. 11 DSC thermograms of melting of PLLA, $PP_{PP\text{-}g\text{-}MAH}$, binary PLLA/$PP_{PP\text{-}g\text{-}MAH}$ and ternary PLLA/$PP_{PP\text{-}g\text{-}MAH}$/INT-$WS_2$ nanocomposites obtained during heating at 10 °C min^{-1} after cooling from the melt to room temperature at 40 °C min^{-1}.

hand, it modifies the double endotherm behaviour observed in the absence of nanofiller. Thus, for neat PLLA, a clear double endotherm can be detected that should be attributed to a melting–recrystallization–melting process of the crystal lamellae originated during the cooling from the melt. In contrast, for the 90/10-INT and 10/90-INT nanocomposites, the endotherm at lower temperature decreases noticeably. In the 50/50-INT sample, the double endotherm could be related to the double exothermic crystallization phenomenon observed during the cooling from the melt, as discussed previously.

When the cooling rate from the melt is increased to 40 °C min^{-1}, the subsequent heating (Fig. 11a and b) shows a melting behaviour with a more pronounced double endotherm, especially in the case of neat PLLA and the blends rich in this component, which can be attributed both to the lower crystallization temperature when the crystals are generated during the cooling and to the lower cold-crystallization temperature during the heating (Table 2), which causes the growth and development of smaller crystals that are more prone to melting–recrystallization–melting processes. Regarding the nanocomposites, since the increase in the cooling rate from the melt makes less important the influence of the heterogeneous nucleation, the melting–recrystallization–melting process has more influence on the subsequent heating, even for the blends rich in $PP_{PP\text{-}g\text{-}MAH}$ and for the neat $PP_{PP\text{-}g\text{-}MAH}$.

3.5. Dynamic mechanical behaviour

In order to obtain information about the effect of INT-WS_2 on the mechanical properties of PLLA/$PP_{PP\text{-}g\text{-}MAH}$ blends, dynamic mechanical properties were measured. Fig. 12 shows the temperature dependence of the storage modulus (E') and loss factor (tan δ) for different PLLA/$PP_{PP\text{-}g\text{-}MAH}$/INT-$WS_2$ formulations. E' and T_g values for all the samples are collected in Table 3. As expected according to the rule of mixtures, E' increases with increasing the PLLA content in the binary PLLA/$PP_{PP\text{-}g\text{-}MAH}$ blends, since the storage modulus of neat PLLA is higher than that of $PP_{PP\text{-}g\text{-}MAH}$. However, the blend with PLLA/$PP_{PP\text{-}g\text{-}MAH}$ ratio of 90 : 10 (*i.e.* 90/10-INT) exhibits higher E' value than pure PLLA, which should be related to the higher crystallinity of this binary mixture compared to that of the neat biopolymer, as revealed by DSC analysis. In fact, two effects determine E' of the blends: the stiffness of the components considering their weight ratio and the overall degree of crystallinity. These effects follow an opposite trend (*i.e.* the former increases while the second drops with increasing $PP_{PP\text{-}g\text{-}MAH}$ concentration), and the overall result depends on the balance of both competing factors. At low $PP_{PP\text{-}g\text{-}MAH}$ contents, the increase in crystallinity probably exceeds the reduction in stiffness induced by the presence of a soft $PP_{PP\text{-}g\text{-}MAH}$ phase, and the

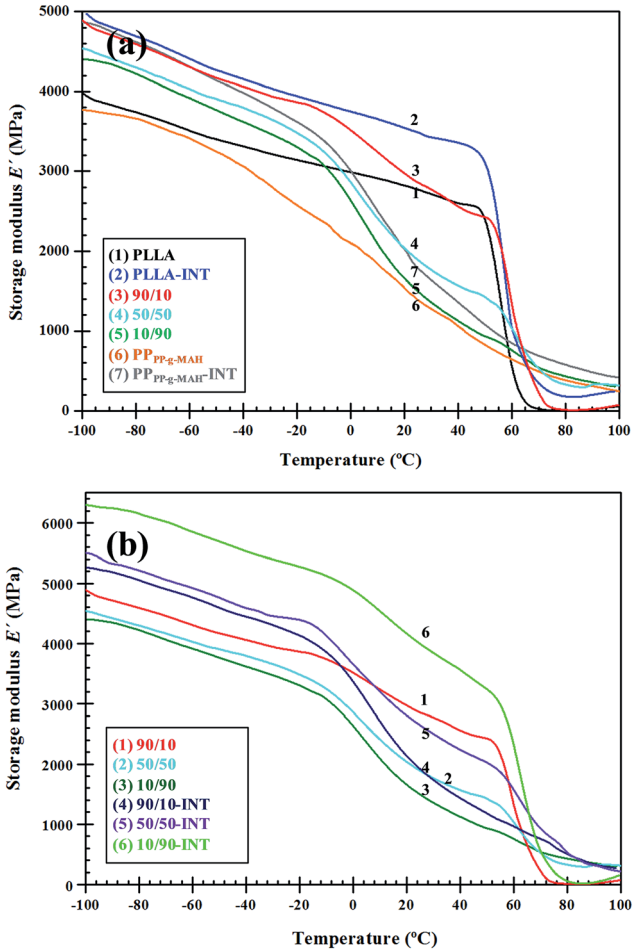

Fig. 12 Evolution of the storage modulus (E') as a function of temperature for (a) PLLA, $PP_{PP\text{-}g\text{-}MAH}$ and different binary systems and (b) PLLA/$PP_{PP\text{-}g\text{-}MAH}$ blends and PLLA/$PP_{PP\text{-}g\text{-}MAH}$/INT-$WS_2$ blend nanocomposites.

Table 3 DMA parameters of different PLLA/$PP_{PP\text{-}g\text{-}MAH}$/INT-$WS_2$ blend nanocomposites based on PLLA, $PP_{PP\text{-}g\text{-}MAH}$ and INT-WS_2[a]

Material	$E'_{25°C}$ (GPa)	T_{g1} (°C)	T_{g2} (°C)
PLLA	2.77	59.8	—
PLLA-INT	3.49	65.1	—
90/10	2.86	68.7	1.2
90/10-INT	4.00	71.7	8.1
50/50	1.90	63.4	3.4
50/50-INT	2.60	66.9	7.5
10/90	1.48	62.3	5.1
10/90-INT	1.88	67.7	13.4
$PP_{PP\text{-}g\text{-}MAH}$	1.36	—	6.5
$PP_{PP\text{-}g\text{-}MAH}$-INT	1.76	—	12.7

[a] E': storage modulus; T_{g1}: glass transition temperature of PLLA and T_{g2}: glass transition temperature of $PP_{PP\text{-}g\text{-}MAH}$.

overall result is an increase in modulus. However, at $PP_{PP\text{-}g\text{-}MAH}$ loadings >10 wt%, the decrease in stiffness dominates, leading to a diminution in E'. On the other hand, the storage modulus of the PLLA/$PP_{PP\text{-}g\text{-}MAH}$/INT-$WS_2$ nanocomposites is systematically higher than those of the corresponding binary PLLA/$PP_{PP\text{-}g\text{-}MAH}$ blends in the whole temperature range, due to the stiffness enhancement through the addition of INT-WS_2 combined with the nucleating role of the inorganic nanotubes. In this case, the synergistic effect of the high INT-WS_2 rigidity[35] and the increase in crystallinity induced by the presence of the inorganic nanotubes contribute to enhance the modulus of the PLLA/$PP_{PP\text{-}g\text{-}MAH}$/INT-$WS_2$ samples. Thus, the room temperature value of $E' = 2860$ MPa for PLLA/$PP_{PP\text{-}g\text{-}MAH}$ (90 : 10) increases by 40% upon addition of 1.0 wt% INT-WS_2 loading (a 44% enhancement in comparison to pure PLLA). This outstanding enhancement is larger than those previously reported for PLLA filled with of other inorganic fillers such as 2 wt% talc or hydroxyapatite (HA),[36] 5 wt% organically modified layered silicate,[37] or 10 wt% polyhedral oligomeric silsesquioxanes (POSS).[38] It is also higher than that found upon addition of organic nanofillers such as 10 wt% thermally reduced graphene (TRG),[39] and comparable to that obtained with the incorporation of 1.0 wt% carbon nanotubes (CNTs) grafted to PLLA,[40] demonstrating the high efficiency of adding small amounts of PP and INT-WS_2 to enhance the modulus of this biopolymer. A slight increment in E' is also observed at temperatures between 80 and 100 °C, which can be attributed to the cold crystallization process occurring during the heating process.

Fig. 13 also compares tan δ data for the different samples. The tan δ peak position represents the T_g of chain segments in the amorphous region. Neat PLLA displays a sharp transition around 60 °C corresponding to its T_g, whereas that of $PP_{PP\text{-}g\text{-}MAH}$ occurs at around 7 °C, showing a broad and small peak. All the binary blends exhibit two T_g, which confirms the formation of a biphasic structure. Interestingly, the T_g of $PP_{PP\text{-}g\text{-}MAH}$ decreases and that of PLLA increases in the blends (Table 3). The decrease in the T_g of the softer phase is probably related to the increase in the amorphous content due to the presence of rigid PLLA, which reduces $PP_{PP\text{-}g\text{-}MAH}$ ability for crystallization, resulting in lower amount of crystals, hence the molecular movement can start at lower temperatures. In contrast, the presence of $PP_{PP\text{-}g\text{-}MAH}$ crystals difficult the mobility of PLLA chains, thereby leading to an increase in the T_g of the stiffest phase. Upon addition of INT-WS_2, both T_g increase in comparison to the values of the binary blends, indicating that the nanofiller imposes restrictions on the mobility of both polymer chain segments. Further, the nanofillers increase the crystallinity of both composite phases, fact that also contributes to the increase in T_g found in the ternary PLLA/$PP_{PP\text{-}g\text{-}MAH}$/INT-$WS_2$ samples. The strongest enhancement is again found for PLLA/$PP_{PP\text{-}g\text{-}MAH}$ (90 : 10), where the T_g of PLLA increases by 9 °C. This T_g increment is comparable to that reported for PLLA/PLLA-*g*-CNT (5 wt%) nanocomposite,[40] although is in contrast to the behaviour reported for PLLA composites filled with nanoclay[37] or POSS,[38] where the T_g was hardly affected by nanofiller incorporation. Besides, the addition of the INT-WS_2 provokes a decrease in the intensity of tan δ, corroborating the constraints on the segmental motion of the polymer chains. Moreover, a low value of tan δ typically indicates more elasticity in a system. Therefore, the lower tan δ in the ternary blend nanocomposites suggests that when the stress is removed, the

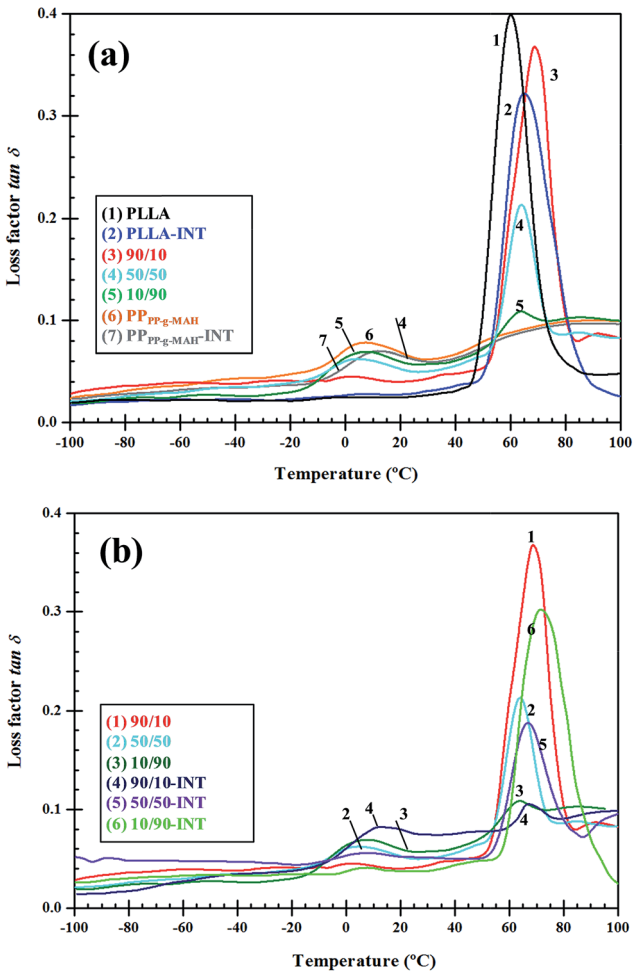

Fig. 13 Evolution of the loss factor (tan δ) as a function of temperature for (a) PLLA, $PP_{PP\text{-}g\text{-}MAH}$ and different binary systems and (b) PLLA/$PP_{PP\text{-}g\text{-}MAH}$ blends and PLLA/$PP_{PP\text{-}g\text{-}MAH}$/INT-$WS_2$ blend nanocomposites.

energy stored in deforming the material is recovered more quickly compared to the corresponding binary PLLA/$PP_{PP\text{-}g\text{-}MAH}$ blends. A broadening of the tan δ peak is also detected, which could be indicative of a more heterogeneous amorphous phase in the nanocomposites compared to the blends, and can also be interpreted as larger volume of the interface. Overall, results demonstrate the suitability of these inorganic nanotubes as fillers for enhancing the mechanical performance of PLLA/$PP_{PP\text{-}g\text{-}MAH}$ blends, and that 90/10-INT displays the optimal combination of high crystallinity, maximum stiffness and glass transition, being its modulus and T_g even higher than that of binary PLLA/INT at a lower cost.

4. Conclusions

In this study, novel PLLA/PP blends with PP-*g*-MAH as a compatibilizer have been reinforced with INT-WS_2 *via* simple melt-blending, and the morphology, thermal and mechanical properties of the resulting hybrid nanocomposites have been characterized. SEM images revealed efficient nanofiller dispersion and modification of the PLLA/PP interface. The addition of INT-WS_2 to the polymeric blends did not significantly influence their thermal stability, except for a small increase in the case of samples rich in PP. The nanofillers were found to exert a nucleating effect on both polymeric components, the effect being more prominent on PLLA and the blends rich in this polymer. This nucleating effect also induced a rise in the crystallization enthalpy and the elimination of the cold-crystallization process. The addition of the INT-WS_2 caused an increase in the storage modulus of the binary blends, attributed to the combination of higher crystallinity and the high INT-WS_2 rigidity. Further, a rise in the T_g of both polymeric components was detected, indicating that the nanofiller imposes restrictions on the mobility of both polymer chain segments. The novel hybrid nanocomposites developed in this work are very promising to be used in the biomedical field.

Acknowledgements

This work was supported by the Spanish Ministry Economy and Competitivity (MINECO), Project MAT2013-41021-P. MN and AD would also like to acknowledge the MINECO for a 'Ramón y Cajal' Senior Research Fellowship.

References

1 L. A. Utracki, *Polymer Alloys and Blends*, Hanser Publishers, New York, 1990.
2 M. M. Reddy, S. Vivekanandhan, M. Misra, S. K. Bhatia and A. K. Mohanty, *Prog. Polym. Sci.*, 2013, **38**, 1653–1689.
3 L. T. Lim, R. Auras and M. Rubino, *Prog. Polym. Sci.*, 2008, **33**, 820–852.
4 K. S. Anderson and M. A. Hillmyer, *Polymer*, 2004, **45**, 8809–8823.
5 B. G. Girija, R. R. N. Sailaja and G. Madras, *Polymer*, 2005, **90**, 147–153.
6 N. Reddy, D. Nama and Y. Yang, *Polym. Degrad. Stab.*, 2008, **93**, 233–241.
7 R. M. Rasal, A. V. Janrkor and D. E. Hirt, *Prog. Polym. Sci.*, 2010, **35**, 338–356.
8 P. Choudhary, S. Mohanty, S. K. Nayak and L. Unnikrishnan, *J. Appl. Polym. Sci.*, 2011, **121**, 3223–3237.
9 N. Ploypetchara, P. Suppakul, D. Atong and C. Pechyen, *Energy Procedia*, 2014, **56**, 201–210.
10 R. Tenne, L. Margulis, M. Genut and G. Hodes, *Nature*, 1992, **360**, 444–445.
11 L. Margulis, G. Salitra, R. Tenne and M. Talianker, *Nature*, 1993, **365**, 113–114.
12 R. Tenne and M. Redlich, *Chem. Soc. Rev.*, 2010, **39**, 1423–1434.
13 A. R. Adini, M. Redlich and R. Tenne, *J. Mater. Chem.*, 2011, **21**, 15121–15231.
14 M. Naffakh, A. M. Díez-Pascual, C. Marco, G. Ellis and M. A. Gómez-Fatou, *Prog. Polym. Sci.*, 2013, **38**, 1163–1231.
15 M. Naffakh and A. M. Díez-Pascual, *Inorganics*, 2014, **2**, 291–312.

16 M. Pardo, T. Shuster-Meiseles, S. Levin-Zaidman, A. Rudich and Y. Rudich, *Environ. Sci. Technol.*, 2014, **48**, 3457–3466.
17 E. B. Goldman, A. Zak, R. Tenne, E. Kartvelishvily, S. Levin-Zaidman, Y. Neumann, R. Stiubea-Cohen, A. Palmon, A. H. Hovav and D. J. Aframian, *Tissue Eng., Part A*, 2015, **21**, 1013–1023.
18 G. Lalwani, A. M. Henslee, B. Farshid, P. Parmar, L. Lin, Y. X. Qin, F. K. Mikos, A. G. Kasper and B. Sitharaman, *Acta Biomater.*, 2013, **9**, 8365–8373.
19 M. Naffakh, C. Marco and G. Ellis, *CrystEngComm*, 2014, **16**, 5062–5072.
20 N. Naffakh and A. M. Díez-Pascual, *J. Mater. Chem. B*, 2014, **2**, 4509–4520.
21 C. Marco, M. A. Gómez, G. Ellis and J. M. Arribas, *J. Appl. Polym. Sci.*, 2002, **84**, 1669–1679.
22 J. B. Zeng, K. A. Li and A. K. Du, *RSC Adv.*, 2015, **5**, 32546–32565.
23 M. Bijarimi, S. Ahmad and R. Rasid. Mechanical, thermal and morphological properties of PLA/PP melt blends. *Proc. Int. Conf. Agric. Chem. Environ. Sci.*, Dubai (UAE), Oct. 6 and 7 2012, pp. 115–117.
24 H. S. Bu, S. Z. D. Chang and R. Wunderlich, *Makromol. Chem., Rapid Commun.*, 1988, **9**, 75–77.
25 E. W. Fischer, H. J. Sterzel and G. Wegner, *Kolloid Z. Z. Polym.*, 1973, **251**, 980–990.
26 T. Miyata and T. Masuko, *Polymer*, 1998, **39**, 5515–5521.
27 P. Pengju, K. Weihua, Z. Bo, D. Tungalag and I. Yoshio, *Macromolecules*, 2007, **40**, 6898–6905.
28 C. Alemán, B. Lotz and J. Puiggalí, *Macromolecules*, 2001, **34**, 4795–4801.
29 J. M. Zhang, Y. X. Duan, H. Sato, H. Tsuji, I. Noda, S. K. Yan and Y. Ozaki, *Macromolecules*, 2005, **38**, 8012–8021.
30 A. Turner-Jones, J. M. Aizlewood and D. R. Beckett, *Makromol. Chem.*, 1964, **75**, 134–158.
31 J. Varga, *J. Macromol. Sci., Part B: Phys.*, 2002, **41**, 1121–1171.
32 W. Xiao, P. Wu and J. Feng, *J. Appl. Polym. Sci.*, 2008, **108**, 3370–3379.
33 M. Naffakh, C. Marco and G. Ellis, *J. Phys. Chem. B*, 2011, **115**, 10836–10843.
34 A. Zak, L. Sallacan-Ecker, A. Margolin, M. Genut and R. Tenne, *Nano*, 2009, **4**, 91–98.
35 I. Kaplan-Ashiri, S. R. Cohen, K. Gartsman, V. Ivanovskaya, T. Heine, G. Seifert, I. Wiesel, H. D. Wagner and R. Tenne, *Proc. Natl. Acad. Sci. U. S. A.*, 2006, **103**, 523–528.
36 X. Liu, T. Wang, M. Yang, L. C. Chow and J. W. Mitchell, *Int. J. Polym. Sci.*, 2014, 827028, 8 pages.
37 K. Prakalathan, S. Mohanty and S. K Nayak, *J. Reinf. Plast. Compos.*, 2012, **31**, 1300–1310.
38 J. M. Raquez, Y. Habibi, M. Murariu and P. Dubois, *Prog. Polym. Sci.*, 2013, **38**, 1504–1542.
39 X. Z. Tong, F. Song, M. Q Li, X. L. Wang, I. J. Chin and Y. Z. Wang, *Compos. Sci. Technol.*, 2013, **88**, 33–38.
40 Y. T. Shieh, G. L. Liu, Y. K. Twu, T. L. Wang and C. H. Yang, *J. Polym. Sci., Part B: Polym. Phys.*, 2010, **48**, 145–152.